Fast neutron measurements with ^{7}Li and ^{6}Li enriched CLYC scintillators

A. Giaz [a,*], N. Blasi [a], C. Boiano [a], S. Brambilla [a], F. Camera [a,b], C. Cattadori [c], S. Ceruti [a,b], F. Gramegna [d], T. Marchi [d,1], I. Mattei [a], A. Mentana [a,b], B. Million [a], L. Pellegri [a,2], M. Rebai [e], S. Riboldi [a,b], F. Salamida [c], M. Tardocchi [f]

[a] INFN Milano, Via Celoria 16, 20133 Milano, Italy
[b] Università degli Studi di Milano, Physics Department, Via Celoria 16, 20133 Milano, Italy
[c] INFN sezione di Milano Bicocca, Piazza della Scienza 3, 20125 Milano, Italy
[d] INFN Laboratori Nazionali di Legnaro, Viale dell'Università, 2, 35020 Legnaro, PD, Italy
[e] Università degli Studi di Milano Bicocca, Physics Department, Piazza della Scienza 3, 20126 Milano, Italy
[f] Istituto di Fisica del Plasma, Associazione EURATOM-ENEA-CNR, Via R. Cozzi 53, 2015 Milano, Italy

ARTICLE INFO

Keywords:
CLYC Scintillator detector
Neutron detection
Fast neutron measurement
Gamma-ray detector

ABSTRACT

The recently developed Cs_2LiYCl_6:Ce (CLYC) crystals are interesting scintillation detectors not only for their gamma energy resolution ($<5\%$ at 662 keV) but also for their capability to identify and measure the energy of both gamma rays and fast/thermal neutrons. The thermal neutrons were detected by the ^{6}Li(n,α)t reaction while for the fast neutrons the ^{35}Cl(n,p)^{35}S and ^{35}Cl(n,α)^{32}P neutron-capture reactions were exploited. The energy of the outgoing proton or α particle scales linearly with the incident neutron energy. The kinetic energy of the fast neutrons can be measured using both the Time Of Flight (TOF) technique and using the CLYC energy signal. In this work, the response to monochromatic fast neutrons (1.9–3.8 MeV) of two CLYC 1″ × 1″ crystals was measured using both the TOF and the energy signal. The observables were combined to identify fast neutrons, to subtract the thermal neutron background and to identify different fast neutron-capture reactions on ^{35}Cl, in other words to understand if the detected particle is an α or a proton. We performed a dedicated measurement at the CN accelerator facility of the INFN Legnaro National Laboratories (Italy), where the fast neutrons were produced by impinging a proton beam (4.5, 5.0 and 5.5 MeV) on a ^{7}LiF target. We tested a CLYC detector ^{6}Li-enriched at about 95%, which is ideal for thermal neutron measurements, in parallel with another CLYC detector ^{7}Li-enriched at more than 99%, which is suitable for fast neutron measurements.

1. Introduction

In the last years several new scintillator materials were developed [1–5]. One class of scintillators, the Elpasolite, discovered approximately 10 years ago, presents excellent performances in terms of gamma and neutron identification and measurement [6–16]. The CLYC (Cs_2LiYCl_6:Ce) crystal belongs to the Elpasolite crystal family, as well as the CLLB ($Cs_2LiLaBr_6$:Ce) and CLLC ($Cs_2LiLaCl_6$:Ce) crystals.

The light yield of CLYC is around 20,000 photons/MeV. It exhibits excellent proportionality between the deposited energy and the light output, which leads to good energy resolution ($<5\%$ at $E_\gamma = 662$ keV) [6–16]. This material is extremely interesting thanks to its capability to identify and measure the energy of both gamma rays and neutrons. The pulse shape discrimination (PSD), based on the measurement of the scintillation decay response, allows an extremely precise identification of neutrons.

The CLYC scintillators can detect both thermal and fast neutrons. The thermal neutron detection capability arises from the presence of ^{6}Li through the reaction ^{6}Li (n,t)α [7,8,10,14,18]. Fast neutrons are detected exploiting the reactions ^{35}Cl (n,p)^{35}S and ^{35}Cl (n,α)^{32}P. These scintillators can therefore be used as a neutron spectrometer since the energy of the outgoing proton or α particle is linearly related to the incoming neutron energy [8,12–15,17,18].

In nuclear physics experiments, especially in case of radioactive beams, there is a great interest in the fast-neutron identification and spectroscopy. Up to now the fast-neutron energy was measured using the time of flight (TOF) technique. As the typical neutron energy in these kinds of experiments ranges from ~1 up to ~10 MeV, the TOF technique requires long flight path (at least

* Corresponding author.
E-mail address: agnese.giaz@mi.infn.it (A. Giaz).
[1] Present address: KU Leuven, Department of Physics and Astronomy, Instituut voor Kern- en Stralingsfysica, Celestijnenlaan 200D, 3001 Leuven, Belgium.
[2] Present address: University of Witwatersrand and iThemba LABS, South Africa.

70 cm) between target and detector. This means that a large number of detectors is required to cover the whole solid angle; in fact, ten times more detectors are required to cover the same solid angle if the detector-target distance is increased from 20 to 70 cm.

The possibility to identify neutrons through PSD and to measure the energy of the fast-neutrons using the detector energy signal, allows a small target-detector distance. Therefore, a small number of detectors are required to cover the whole solid angle. In summary, the characteristics of CLYC scintillators make them good candidates for nuclear physics experiments in which the fast-neutron and γ-ray identification and spectroscopy is needed [20–22].

Few works [15,17–19] were already published to study the CLYC response to neutrons. They used monochromatic neutron beams in the range 0.4–14 MeV, and they showed that each neutron energy above ∼2.5 MeV produces a structured spectrum due to the different allowed reaction channels. In ref. [17], monochromatic neutrons in the energy range 0.4–4.7 MeV were measured and the linear relation between the neutron energy and the alpha or proton energy was demonstrated. Ref. [15] confirmed the linearity and showed a neutron energy resolution of 7.5–10.5%, rather constant with neutron energy. Such resolution is larger than that expected for equivalent γ-rays. Note that to obtain the same energy resolution with TOF, we should place the detectors at ∼1 m distance, taking into account our measured timing resolution of 2 ns. Refs. [15,23] show that neutrons with energies higher than 8 MeV induce different reaction channels and the possibility to populate excited states making therefore quite difficult the measurement of their kinetic energy.

All these results show that the neutron induced direct reactions on ^{35}Cl provide a promising mechanism for the identification and spectroscopy of fast neutrons with energy between 1 and 8 MeV. The presence of ^{6}Li in the CLYC crystal gives rise to a thermal neutron peak, leading to a limitation in sensitivity for fast neutron spectroscopy. Indeed, in the energy range 3.0–3.5 MeVee, the ^{6}Li thermal peak and the ^{35}Cl(n,p)^{35}S peak overlap, thus making spectroscopy impossible, whereas the use of a ^{7}Li enriched crystal allows a fast neutron spectroscopy in the energy range (1–8 MeV) as ^{7}Li is insensitive to thermal neutrons.

Despite these promising results, the fact that the neutron spectrum has a structured shape above ∼2.5 MeV, which strongly depends on the neutron energy, makes quite difficult to use these crystals in realistic nuclear physics experiments, where the neutron energy to be detected is normally a continuum.

The aim of this work is to develop a method to disentangle both the contributions of neutrons with different energies and neutrons with the same energy undergoing different reaction channels.

In general, the combined use of TOF, PSD and direct energy measurement provides a very powerful tool for the neutron identification and measurement. It allows, (i) the separation between fast and thermal neutrons (ii) the possibility to have two independent measurements of neutron energy and (iii) the identification of neutron induced protons (from the reaction ^{35}Cl(n, p)^{35}S) and neutrons induced α particles (from the reaction ^{32}Cl(n, α)^{35}P). This last feature gives the unique possibility to measure continuous neutron spectra without any kind of unfolding procedure. It is also important to note that in this case the use of TOF does not imply a large distance between target and detectors, since the energy resolution would be given by the CLYC resolution.

In this work we study the response to monochromatic fast neutrons of two cylindrical 1″ × 1″ samples of a CLYC scintillator, the first enriched with more than 99% of ^{7}Li (CLYC-7) and the second one enriched with ∼95% of ^{6}Li (CLYC-6). The time information provided by CLYC (which is of the ns order [14]) was exploited to measure, in an independent way from the direct neutron energy measurement, the energy of the neutrons. In the experiment we acquired both the time and the energy information and we combined the two observables to separate the different neutrons induced reaction channels. The experimental set-up details can be found in Section 2. The analysis of fast-neutron measurements, performed with both detectors and with two different acquisition systems are reported in Section 3. The fast neutron energy, deduced from TOF technique and energy signal, is reported in Section 4. The conclusion of the work are in Section 5.

2. Experimental set up

The experiment, performed at the CN facility of Legnaro National Laboratories (LNL), Italy, aimed at the study of the fast-neutron response of two cylindrical 1″ × 1″ samples of CLYC scintillator, one with more than 99% enrichment of ^{7}Li and one with ∼95% enrichment of ^{6}Li [23]. During the measurement, the pulsed beam allowed the measurement of the neutron energy using two different techniques, exploiting the energy spectroscopy capability of the CLYC scintillator and the standard TOF method.

The neutron flux was produced, through the reaction ^{7}Li(p, n)^{7}Be, impinging a pulsed proton beam (3 MHz rep rate, ∼2 ns pulse width) on a ^{7}LiF target 700 μg/cm^{2} thick. Different proton beam energies (4.5–5.0–5.5 MeV) were used to produce monochromatic neutrons in the energy range of 1.9–3.8 MeV. The two CLYC detectors were placed at 77 cm from the target to have a rather long flight path for TOF measurements, for a reasonable separation of neutrons through the TOF measurements. The

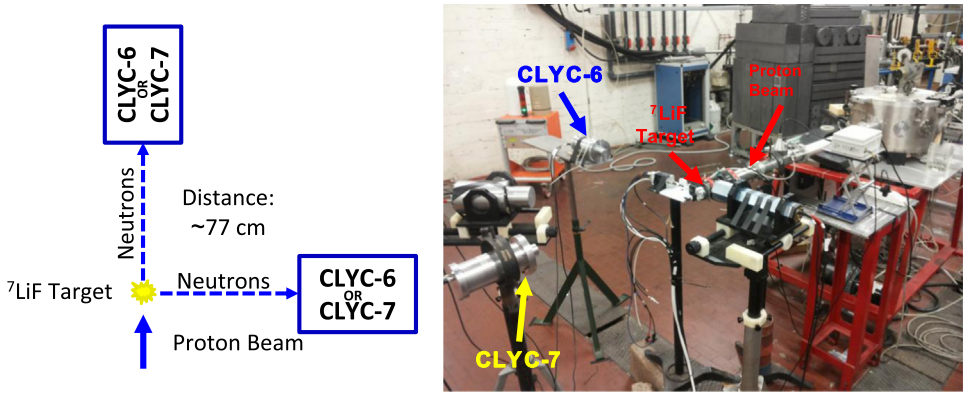

Fig. 1. Left panel: the schematic view of the experimental set-up. The proton beam impings on a ^{7}LiF target. The emitted neutrons are detected by the two CLYC scintillators that are placed at 0° and 90° degrees. Right panel: a picture of the experimental set up.

Table 1
Column 1 reports the proton energies, column 2 reports the detector position and column 3 the corresponding neutron energies.

Proton energy (MeV)	Detector position (deg.)	Neutron energy (MeV)
4.5	0	2.8
4.5	90	1.9
5.0	0	3.3
5.0	90	2.3
5.5	0	3.8
5.5	90	2.7

detector were also placed at 0° and 90° from the beam direction to measure different neutron energies with the same proton beam energy. A picture and a scheme of the experimental set-up are shown in Fig. 1. The emitted neutrons have an angular distribution which is not isotropic, but the variation in neutron energy is smaller than ~0.06 MeV within 2°, which is the angle subtended by the detectors placed at 77 cm distance. Therefore the measured neutrons can be considered monochromatic. Six neutron energies, reported in the third column of Table 1, were measured for each detector.

The two CLYC scintillators were coupled to HAMAMATSU R6233-100Sel photomultiplier tubes (PMT) and to two standard HAMAMATSU E1198-26 and E1198-27 voltage dividers (VD). The PMTs were powered at 800 V.

Two different acquisition systems were used; the first one was a standard analog acquisition system and the second one was completely digital. An active splitter was used to provide two amplified copies of the anode signal (gain of a factor 6) to both acquisition systems. For the analog acquisition system, a copy of the anode signal was formed with a 16 channel NIM module, called BAFPRO [26], developed by the electronic group of the university of Milan. This module was modified to be used with CLYC scintillators by changing the shaping time to approximately 2 μs, the formed signal (called 'slow') was sent to a CAEN VME-ADC. The time spectra were obtained using a CFD (inside the modified BAFPRO unit) with a fix shaping delay of 8 ns and a CAEN VME-TDC. The BAFPRO unit provides also a signal proportional to the maximum amplitude of the anode signal (called 'fast' signal). The PSD, between gamma rays and neutrons, was performed producing a fast vs slow matrix. Data were acquired using a DAQ in a KMAX environment [27].

When using the digital acquisition system, the anode signal was digitized with a 12 bit, 600 MHz LeCroy waverunner HRO 66Zi oscilloscope.

For both the acquisition systems, the trigger of the experiment was the coincidence between the OR of the two detectors and the pulsed beam signal. The latter provided a time resolution of ~4 – 6.5 ns.

The analog acquisition system underwent a smaller dead time than the digital one, therefore the analog acquisition system allowed to acquire more statistics. The digital acquisition system provided a better separation between the gamma rays and the neutrons, especially at low energies, and it offered the possibility to work offline with the acquired pulses (pile up rejection, signal filtering, etc.).

3. Neutron identification and measurement

The neutron detection capability mainly arises from the presence of ^{6}Li and ^{35}Cl atoms in the crystal. The ^{6}Li isotope absorbs thermal neutrons with a cross-section of 940 barns via the reaction ^{6}Li(n,t)α [24,25] (Q-value E=4.783 MeV) and fast neutrons with a cross-section of the order of 0.2 barns at $E_n \approx 3$ MeV

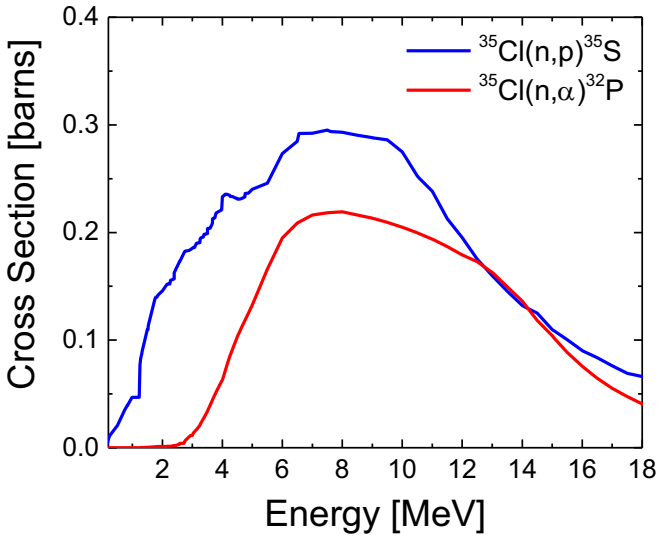

Fig. 2. The cross-section of ^{35}Cl neutron-capture reactions [24].

[24,25]. The Q-value of the reaction ^{35}Cl(n,p)^{35}S is 0.615 MeV, while for ^{35}Cl(n,α)^{32}P is 0.937 MeV. The cross-sections for thermal neutrons on ^{35}Cl are of the order of 0.5 barns for the (n,p) reaction and 5 10^{-4} barns for the (n,α) reaction. As these cross-sections are rather small, if compared to those of the ^{6}Li, the presence of ^{35}Cl is important mainly for fast neutrons detection. In the case of fast neutrons (e.g. E_n~3 MeV), the cross-sections of ^{35}Cl are of the order 0.2 for ^{35}Cp(n,p)^{35}S and 0.02 barns for ^{35}Cl(n,α)^{32}P (see Fig. 2). Similar values were reported also in [17,24]. The cross-section for the reaction ^{35}Cl(n,p)^{35}S increases as the neutron energy raises up to 8 MeV, while the cross-section of the ^{35}Cl(n,α)^{32}P reaction is significant only for neutron energies higher than 2.5 MeV. Refs. [15,17] measured the peak induced by the alpha particles from the ^{35}Cl(n,α)^{32}P reaction at E_n~2.5 MeV.

These numbers show that the cross-section for fast-neutron capture on ^{6}Li is comparable with that on ^{35}Cl. However, since Q-values are very different, we expect very different deposited energies in the crystal.

The thermal neutron efficiencies of both the CLYC-6 and CLYC-7 detectors, used in these measurements, were characterized in a previous work [23]. For the ^{7}Li enriched CLYC crystal an efficiency to thermal neutrons of ~0.3% with respect to the ^{6}Li enriched CLYC was measured. In fact, the presence of ^{6}Li in the CLYC-6 sample induces the thermal neutron peak at 3.0–3.5 MeV. This constitutes a huge background when focused on fast-neutron detection (the cross-section on ^{6}Li is ~1000 larger than the cross-section on ^{35}Cl reactions).

In the following subsections we report the analysis of the acquired data with the two detectors and the two acquisition systems: data recorded with CLYC-7 and CLYC-6 acquired with the digital acquisition system are presented in Sections 3.1 and 3.2, respectively, and data acquired using the analog DAQ system for CLYC-7 and CLYC-6 are both discussed in Section 3.3.

3.1. Fast neutron identification and measurement with the CLYC-7 scintillator and the digital acquisition system

The neutron gamma discrimination was performed integrating the signals within two different windows as described in ref [23]: the first one (W1) from the onset of the signal to 80 ns, the second one (W2) from 100 ns to 600 ns. The PSD ratio R was defined as: R=W2/(W2+W1). A matrix was created placing on the y axis the PSD ratio and on the x axis the total deposited energy (integrating the signals for 3 μs). A standard digital CFD algorithm was used to

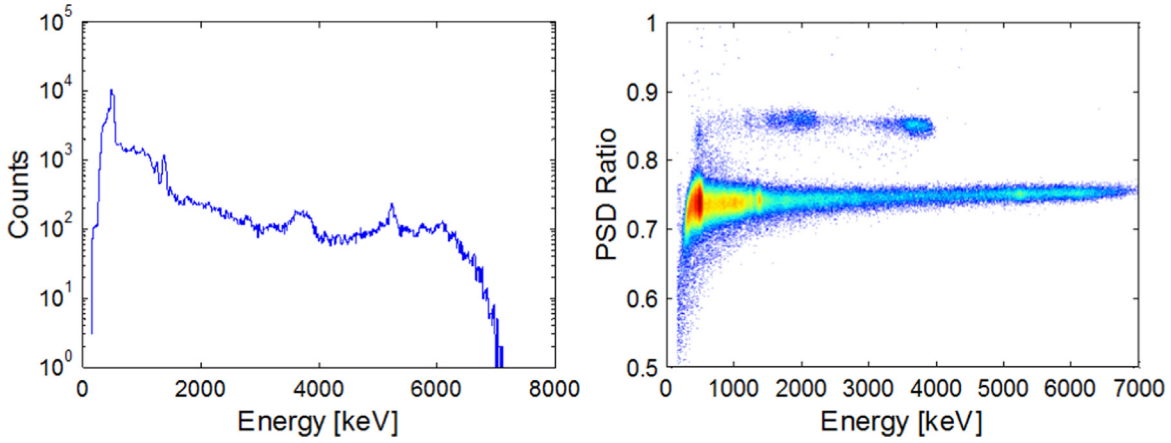

Fig. 3. CLYC-7 data for $E_n = 3.3$ MeV. Left panel: the total energy spectrum measured during the experiment. Neutrons are not visible due to the backgrund. Right panel: the PSD matrix measured during the experiment. The neutron peaks from the reaction $^{35}Cl(n,p)^{35}S$ and the one related to $^{35}Cl(n,\alpha)^{32}P$, are visible at PSD of 0.85 and $E \sim 3.8$ MeV and $E \sim 2.0$ MeV, respectively. The logarithm of the counts of the matrix is plotted on the z axis.

provide the time information. The CFD shaping delay was 4 ns and a linear interpolation was used to extract the zero crossing of the signal.

The results reported in Figs. 3 and 4 were obtained with the CLYC-7 detector placed at 0° and a proton beam energy of 5.0 MeV which corresponds to $E_n = 3.3$ MeV. The total energy spectrum is shown in the left panel of Fig. 3. The neutron peaks are not visible because of the large background. The major source of background consists of prompt and delayed γ-rays induced by the interaction of the neutrons with the materials surrounding the crystal (e.g. the aluminium case). In the right panel of Fig. 3 the measured PSD matrix is displayed. The neutron peaks from the two capture reactions on ^{35}Cl are clearly visible at PSD ~ 0.85 and $E \approx 2$ and ≈ 3.8 MeV. Fig. 4 shows the correspondent time vs energy matrix with (right panel) and without (left panel) a condition on the PSD ratio ($0.8 < \text{PSD ratio} < 0.9$). Fig. 4 shows that the selection on TOF (86–100 ns) cannot discriminate between neutrons or delayed gamma rays, while the PSD allows neutron identification. When only neutron-capture reactions on ^{35}Cl are present, the PSD techniques are sufficient to identify and measure the neutron energy. In a more general case of a neutron continuous spectrum both conditions are useful.

The neutron spectra of the six setups of Table 1 are show in Fig. 5. The peak related to the reaction $^{35}Cl(n,\alpha)^{32}P$ appears in only four panels of Fig. 5, but it is more intense in the right-bottom one because of the cross-section as shown in Fig. 2.

3.2. Fast neutron identification and measurement with the CLYC-6 scintillator and the digital acquisition system

In this section the results of the data recorded using the CLYC-6 scintillator are presented following the same scheme of Section 3.1. The spectra shown in Figs. 6 and 7 are relative to neutron energy of 3.8 MeV. The measured energy spectrum is shown in the left panel of Fig. 6. As for the left panel of Fig. 3, the fast-neutrons peaks are embedded in a huge background. The thermal neutron peak is visible around 3.2 MeVee. In the right panel of Fig. 6 the PSD matrix is shown. At the PSD ratio of 0.85 there are three neutron peaks, the most intense is due to thermal neutrons, while the other two peaks are related to the neutron-capture reactions on ^{35}Cl.

For the CLYC-6 detector the condition on the PSD ratio is not sufficient to select fast neutron events. The energy spectrum obtained by gating on PSD values corresponding to neutron events is dominated by thermal neutrons, as shown in Fig. 7. The selection on TOF becomes fundamental to disentangle fast-neutrons from thermal neutrons. The left and the right panel of Fig. 8 show the time vs energy matrix, with and without the PSD ratio gate. For the CLYC-7 detector only the two peaks of the neutron capture reaction on ^{35}Cl were visible while for the CLYC-6, a vertical structure at ~3.2 MeV and a structure between 5.5 and 7.5 MeV emerged. Both structures are produced by reactions with ^{6}Li: the first is due to thermal neutron capture, while the second is due to the fast-neutron capture. The selection of the neutrons on both the

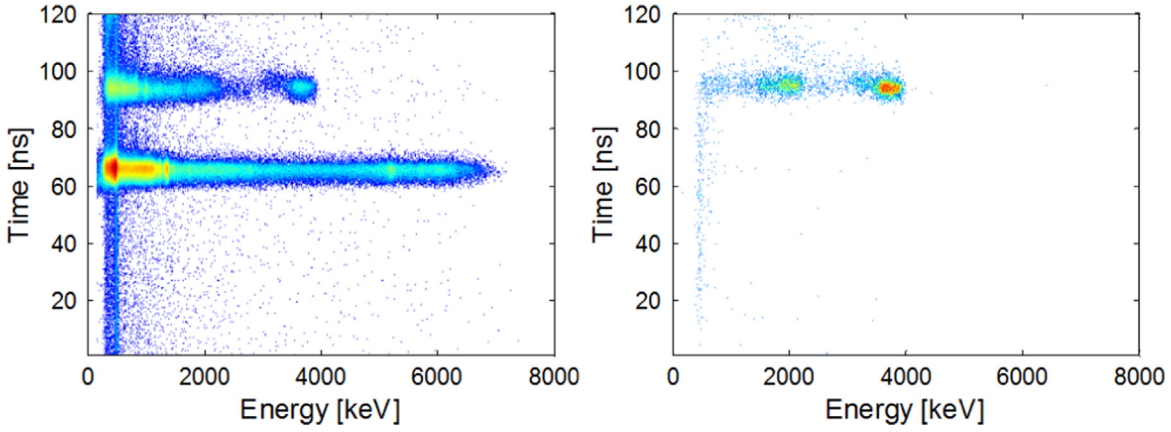

Fig. 4. Left panel: the time vs energy matrix. The line at 70 ns corresponds to the prompt events, while the line at 95 ns to the delayed events. Right panel: the same matrix of the left panel, but with a gate on the PSD ratio (0.8–0.9). In this case only the delayed peak is present. The logarithm of the counts of the matrixes is plotted on the z axis. The z scales of the two plot are different.

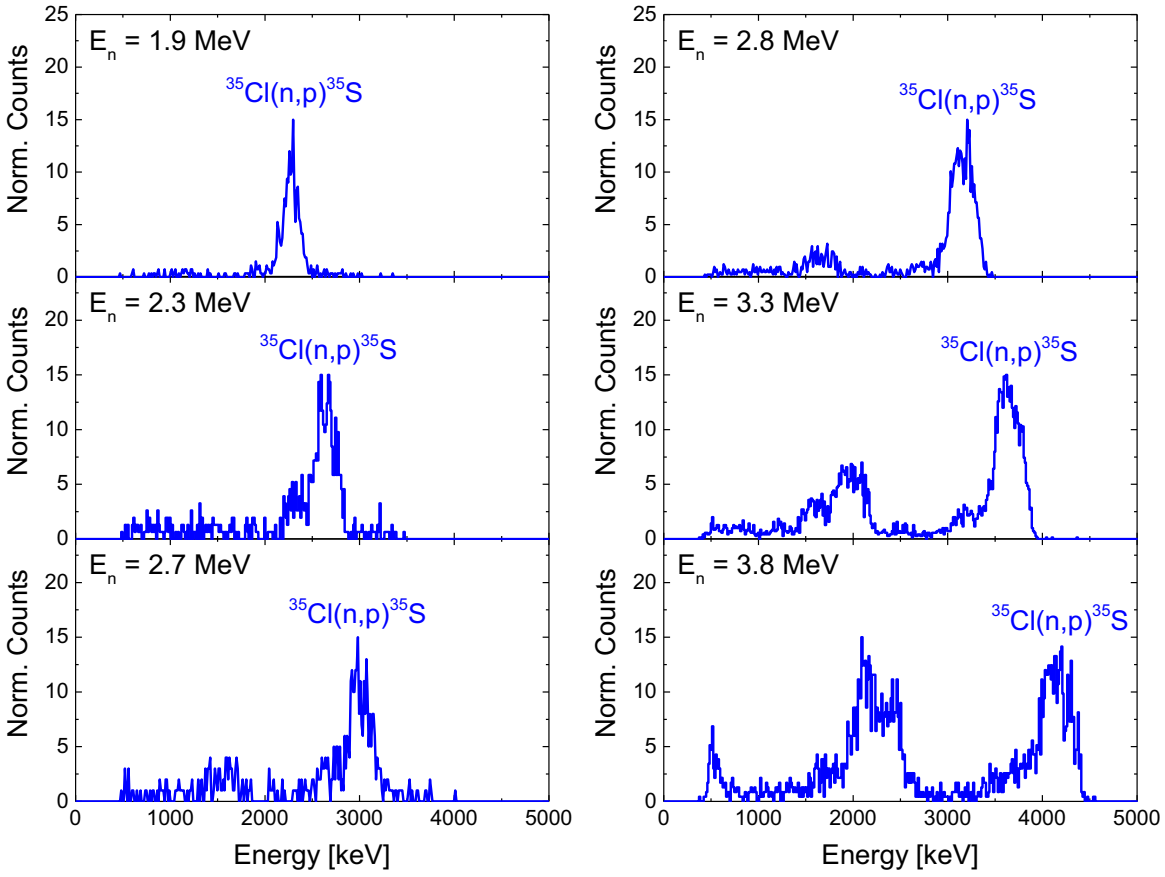

Fig. 5. The neutron energy spectra measured using the CLYC-7 detector are shown. Both PSD and TOF gates are active. Spectra are normalized at the maximum counts. The peak at higher energies corresponds to the population of the ^{35}S ground state in the ^{35}Cl(n,p) reaction, while the structures at ~1.7 MeV in the left bottom panel and more clearly visible at ~2, 2.3 MeV in the right panels contain contributions from the excited states of ^{35}S and the ^{32}P ground and excited states from the ^{35}Cl(n,α).

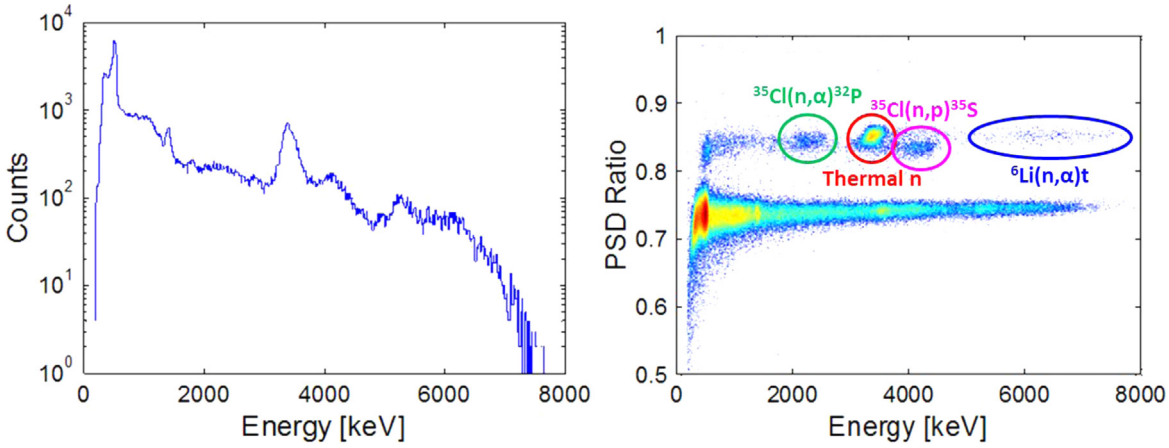

Fig. 6. CLYC-6 data at E_n=3.8 MeV. Left panel: the energy spectrum measured during the experiment. The fast-neutron peaks are not visible owing to the backgrund. Right panel: the measured PSD matrix. The neutron peak from the reaction ^{35}Cl(n,p)^{35}S (magenta circle), the one related to ^{35}Cl(n,α)^{32}P and to contributions from the excited states of ^{35}S (green circle), the thermal neutron peak (red circle), and the fast neutrons captured by ^{6}Li (blue circle) are clearly visible. The logarithm of the counts of the matrix is plotted on the *z* axis. (For interpretation of the references to color in this figure legend, the reader is referred to the web version of this article.)

PSD and the TOF produces a neutron spectrum where the thermal neutron contribution is strongly reduced but not eliminated (see Fig. 9).

The selection of the neutrons on both the PSD ratio ($0.8 < \text{PSD ratio} < 0.9$) and the TOF ($80\ \text{ns} < \text{TOF} < 94\ \text{ns}$) produces a neutron spectrum where the thermal neutron contribution is strongly reduced but not eliminated. The neutron spectra corresponding to the six neutron energies listed in Table 1 are shown in Fig. 9. One can see that for both the fast neutron energies E_n=2.8 and E_n=3.3 MeV thermal neutron and fast-neutron peaks overlap. The thermal neutron peak is indicated by a red line in Fig. 9.

The thermal neutron contribution can be subtracted using the TOF information. The left panel of Fig. 10 shows a zoom of the time vs energy matrix of the region corresponding to the neutron induced events in case of beam energy of 4.5 MeV and the detector at 0°. Two different regions in TOF were selected: the first one (region A) is centered around the neutrons TOF, while the second (region B), with the same dimensions as the first one, contains

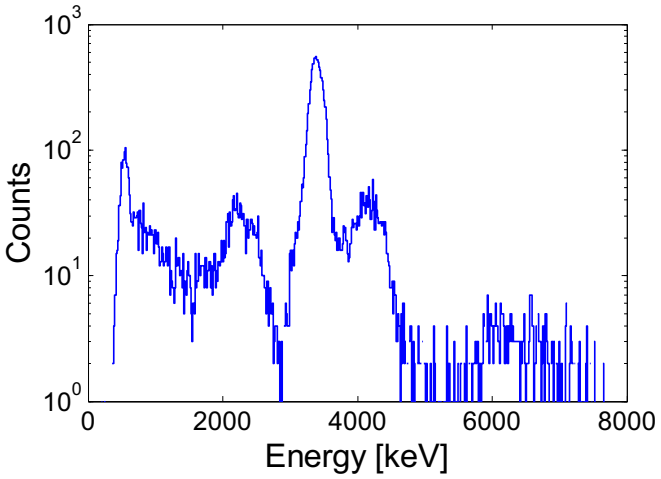

Fig. 7. The expected neutron energy is 3.8 MeV. The energy spectrum obtained by selecting the neutrons by the PSD ratio ($0.8 < \text{PSD ratio} < 0.9$). The two peaks related to the neutron-capture reactions on ^{35}Cl are visible around 2.5 and 4.0 MeV, but the dominant contribution in the spectrum is the thermal neutron peak located at $\sim$3.2 MeV.

only random coincidences with thermal neutrons at higher time values (see black and red boxes in the left panel of Fig. 10, respectively). The spectra obtained with these gates are shown in the right panel of Fig. 10. The black line indicates the spectrum obtained with the gate on region A, and includes both the fast and thermal neutrons, while the red line spectrum, gated on region B, includes only the thermal neutrons. The blue line spectrum is obtained as the difference between the red and the black and it corresponds to the E_n=2.8 MeV neutrons only.

3.3. Fast neutron identification and measurement with CLYC-7 and CLYC-6 scintillators and analog acquisition system

The same procedure of the previous sections was applied to the data acquired with the analog acquisition system. The spectra, reported in Fig. 11, are for CLYC-7 detector placed at 0° and a proton beam energy of 5 MeV. In the top-left panel of Fig. 11, the fast vs slow matrix is shown. The modified BAFPRO unit provides two signals: the first one is proportional to the signal amplitude and the second one is proportional to the deposited energy (see Section 2). The fast vs slow matrix allows to separate between gamma rays and neutrons. With the analog acquisition system the gamma-neutron separation at low energies is not as good as in the case of the digital acquisition system. The TOF vs the energy matrix obtained after the selection on neutron in the fast vs slow matrix, is shown in the bottom-left panel of Fig. 11. The fast neutron spectrum was obtained by gating on neutrons both in the PSD and in the TOF spectra, and it is shown in the bottom right panel of Fig. 11. The two peaks corresponding to the neutron-capture reactions on ^{35}Cl are visible. Taking into account that the acquired statistic with the analog acquisition system is about 10 times larger than the statistic acquired with the digital acquisition system, one can see that the two neutron spectra of Fig. 5, right-middle panel, (digital system) and of Fig. 11, right-bottom panel, (analog system) are similar.

Similar results were observed in the case of the CLYC-6 detector and an example is shown in Fig. 12. As for the digital approach, the selection on neutrons is not sufficient to eliminate the thermal neutron events (see top-right panel of Fig. 12). In this case the selection on TOF is fundamental to reduce the thermal neutron background. The fast neutron spectrum shown in bottom-right panel of Fig. 12 is obtained with both the selections on neutrons on PSD and on TOF. The two peaks of the neutron-capture reactions on ^{35}Cl are now clearly visible. The neutron spectra at the six different energies measured during the experiment are shown in Fig. 13. In the spectra, the thermal-neutron background was subtracted in the same way as for the digital acquisition system (Section 3.2).

4. Neutron energy measurement

In this section we discuss the measurement of the neutron energy and the neutron energy resolution, focusing on the TOF technique in Section 4.1 and the direct use of the energy signal in Section 4.2.

4.1. The TOF technique

The well-established TOF technique can be used to reconstruct the neutron energy spectrum exploiting timing information from the acquired signals.

The CLYC crystal, with an optimized PMT and electronics, has an intrinsic sub-nanosecond time resolution [14]. The time resolution of the detectors used in this work, is $\sim$ 2 ns. The time resolution measured during the experiment was dependent on the beam time quality, and it varied between 4.0 and 6.5 ns, as shown in Fig. 14.

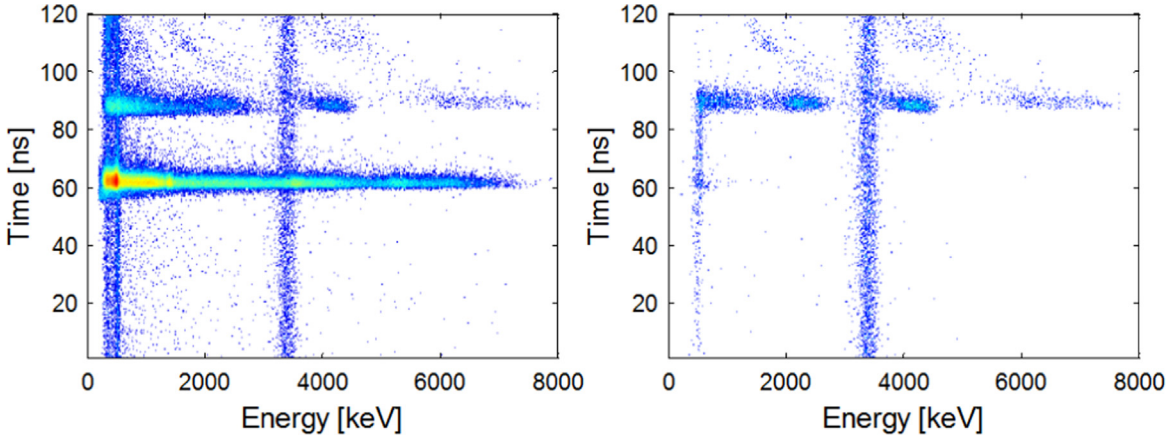

Fig. 8. The expected neutron energy is 3.8 MeV. Left panel: the time vs energy matrix measured during the experiment. The line at 65 ns corresponds to the prompt events, while the line at 90 ns corresponds the delayed events. Right panel: the same matrix of the left panel, but with a gate on the neutrons in the PSD ratio ($0.8 < \text{PSD ratio} < 0.9$). In this case only the delayed events and the vertical structure at 3.2 MeV (thermal neutrons) are present. A small structure is also present at energies between 5.5 and 7.5 MeV, related to fast neutrons captured by ^{6}Li. The logarithm of the counts of the matrixes is plotted on the *z* axis.

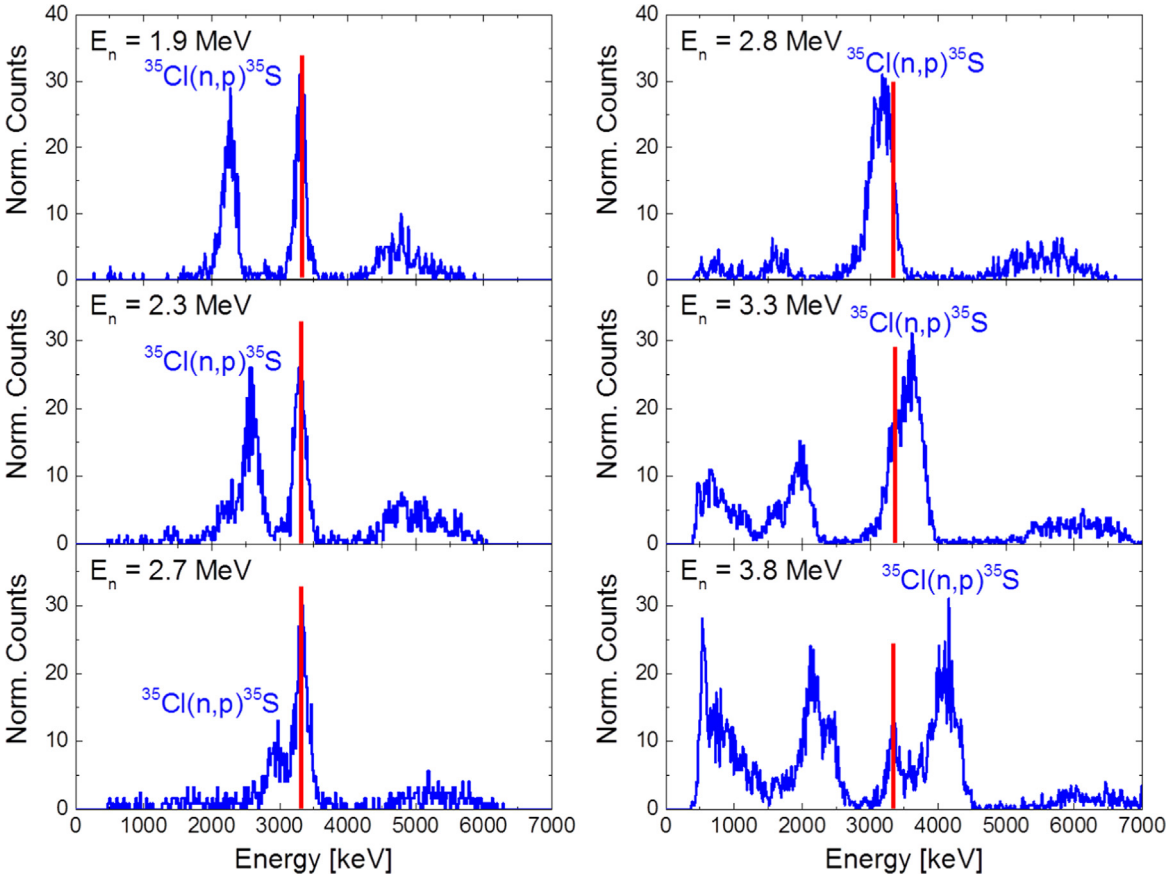

Fig. 9. The measured neutron energy spectra of the CLYC-6 detector. The measured neutron energies are indicated in the plots. The thermal neutron peak is highlighted with a red line in all panels. The spectra are normalized to the maximum number of counts. In the left panels the detector was at 90°, while in the right ones was at 0°. It is important to point out that the thermal and fast neutron ratio is not constant for panels. The peak at higher energies corresponds to the population of the ^{35}S ground state in the ^{35}Cl(n,p) reaction, while the structure at energies ~2 MeV lower contains contributions from the excited states of ^{35}S and the ^{32}P ground and excited states from the ^{35}Cl (n,α). (For interpretation of the references to color in this figure legend, the reader is referred to the web version of this article.)

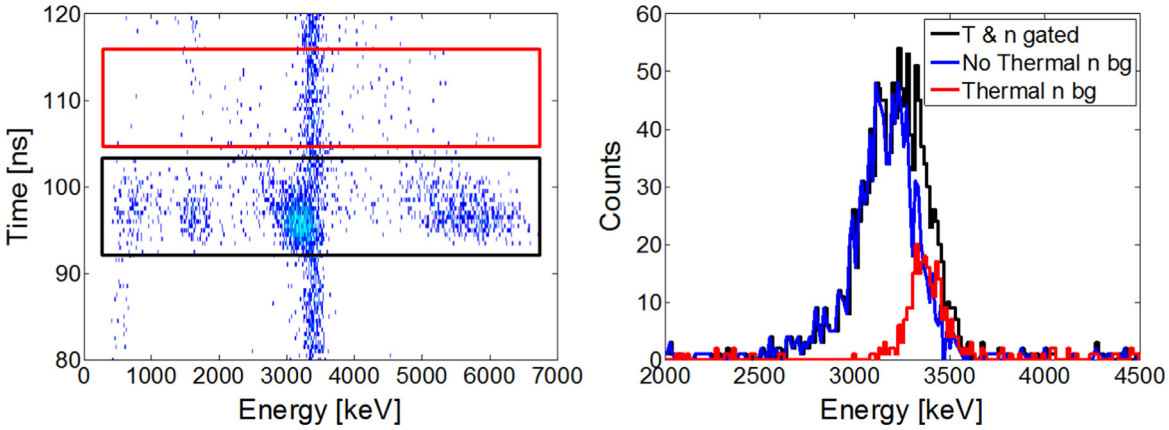

Fig. 10. Left panel: the time vs energy matrix measured with CLYC-6 at 0° and a proton beam of 4.5 MeV. The black and the red boxes indicate the gate on TOF used to produce the black line and the red line spectra shown in the right panel, respectively. The logarithm of the counts of the matrix is plotted on the *z* axis. Right panel: the black line spectrum includes both the fast neutrons and the thermal neutrons, the red line spectrum includes only the thermal neutrons, the blue line spectrum is the difference between the black and the red one. The blue spectrum corresponds to the E=2.8 MeV neutron spectrum with the thermal neutron background subtracted. (For interpretation of the references to color in this figure legend, the reader is referred to the web version of this article.)

Two peaks are present in the TOF spectra of Fig. 14: the larger one is the prompt peak and the other is the delayed one. The prompt peak is related to the gamma rays emitted in the proton induced reaction on the target, while the delayed peak is related to neutrons and delayed γ-rays. The centroid position of the time peak allows to extract the TOF of neutrons and consequently their energy. The TOF centroids of the delayed peak measured for the six energies of Table 1, for both detectors and for both acquisition systems, are plotted in Fig. 15. They are in good agreement with the expected TOF values (dashed line).

If the neutron energy is not known from TOF it will be possible to extract the neutron energy by using the following formula:

$$E_{\mathrm{n}} = \frac{1}{2} m_{\mathrm{n}} \left(\frac{d}{\mathrm{TOF_n} - \mathrm{TOF_\gamma} + \frac{d}{c}} \right)^2$$

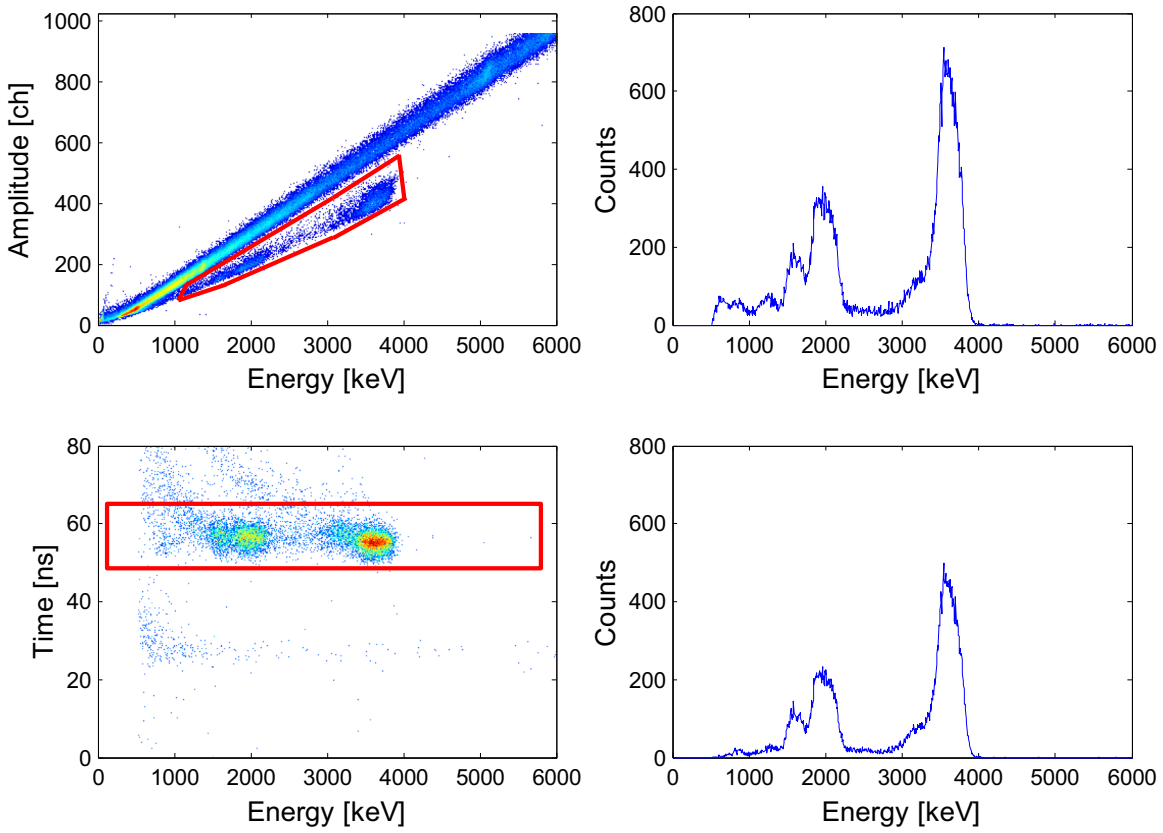

Fig. 11. In all panels, the CLYC-7 detector was placed at 0° and the beam energy was 5 MeV. Top-left panel: the fast vs slow matrix. The red box is the graphical cut used to select the neutrons. The logarithm of the counts of the matrix is plotted on the *z* axis. Top-right panel: the energy spectrum obtained with the gate on neutrons in the fast vs slow matrix. Bottom left panel: the time vs energy matrix obtained gating on neutrons in the amplitude vs energy matrix. The red box indicates the selection on time. The logarithm of the counts of the matrix is plotted on the *z* axis. Bottom-right panel: the fast neutron spectrum obtained after the two selections shown in the left panels. The two peaks corresponding to the neutron capture on ^{35}Cl are clear visible. (For interpretation of the references to color in this figure legend, the reader is referred to the web version of this article.)

where d is the distance between the target and the detector, m_n is the neutron mass, c is the speed of light, TOF_n is the measured TOF for neutron and TOF_γ is the gamma ray TOF.

4.2. CLYC scintillator energy signal

The big advantage of the CLYC detectors is that the neutron energy can be extracted also directly from the deposited energy spectra that are shown in Fig. 13. From the gated energy spectra it is possible to extract the peak centroid positions which correspond to the neutron energy plus the Q-value of the reaction ^{35}Cl(n,p)^{35}S. The measured fast-neutron energy is linearly related to the incident neutron energy, as shown in Fig. 16. The measured energy is always slightly smaller than the expected one for gamma rays. This effect can be explained with the presence of a quenching factor as already show in [17]. The measured quenching factor (defined as the ratio between the measured neutron energy and the expected one) ranges from 0.85 up to 0.92.

The fast-neutron energy resolution obtained in all the data (both CLYC-6 and CLYC-7, both analog and digital acquisition system, for the six measured energies) are plotted as a function of neutron energy in Fig. 17. It ranges between 7.5% and 10.2%. The thermal neutron background in the CLYC-6 spectra was subtracted using TOF. Similar values for the fast-neutrons energy resolution were found also in [15]. The measured energy resolution is larger than the one expected for gamma rays of the same energy. The reason of that is not clear and a detailed study of the reaction mechanism is needed.

The possibility to identify neutrons and measure their energy directly from the signal is a crucial aspect in nuclear spectroscopy experiments, in which the distance between the detector and the target limits the γ-ray efficiency of the detector array.

4.3. Measurement of a neutron continuous spectra using TOF and energy signal

The combination of the two techniques provides a better identification of the neutrons and a better measurement of their energy, especially for the CLYC-6 detector. Each technique has advantages and disadvantages, as previously discussed. In Fig. 18, the measured time vs energy matrixes of five of the six neutron energies measured during the experiment (see Table 1) is shown. The 2.7 MeV energy was not taken into account since very close to the 2.8 MeV one. Neutrons were selected using the PSD ratio. Five spots on a diagonal line are clearly visible, they are highlighted by lines connecting their centroids with the associated time and energy. The spots correspond to the neutrons detected with the reaction ^{35}Cl(n,p)^{35}S. A second diagonal line (indicated by a magenta box in Fig. 18) is related to the neutrons detected with the reaction ^{35}Cl(n,α)^{32}P. The matrix for the CLYC-6 detector is not shown because of the thermal neutron background. In the case of a continuum-neutron spectrum the combination of the two pieces of information will allow the separation of the different reaction channels.

The combination of these two techniques will be very useful in case of more complicated situations, as can occur in nuclear physics experiments, in which several neutrons and gamma rays with different energies can be emitted. A matrix like the one of Fig. 18 can provide information about the time and energy correlation

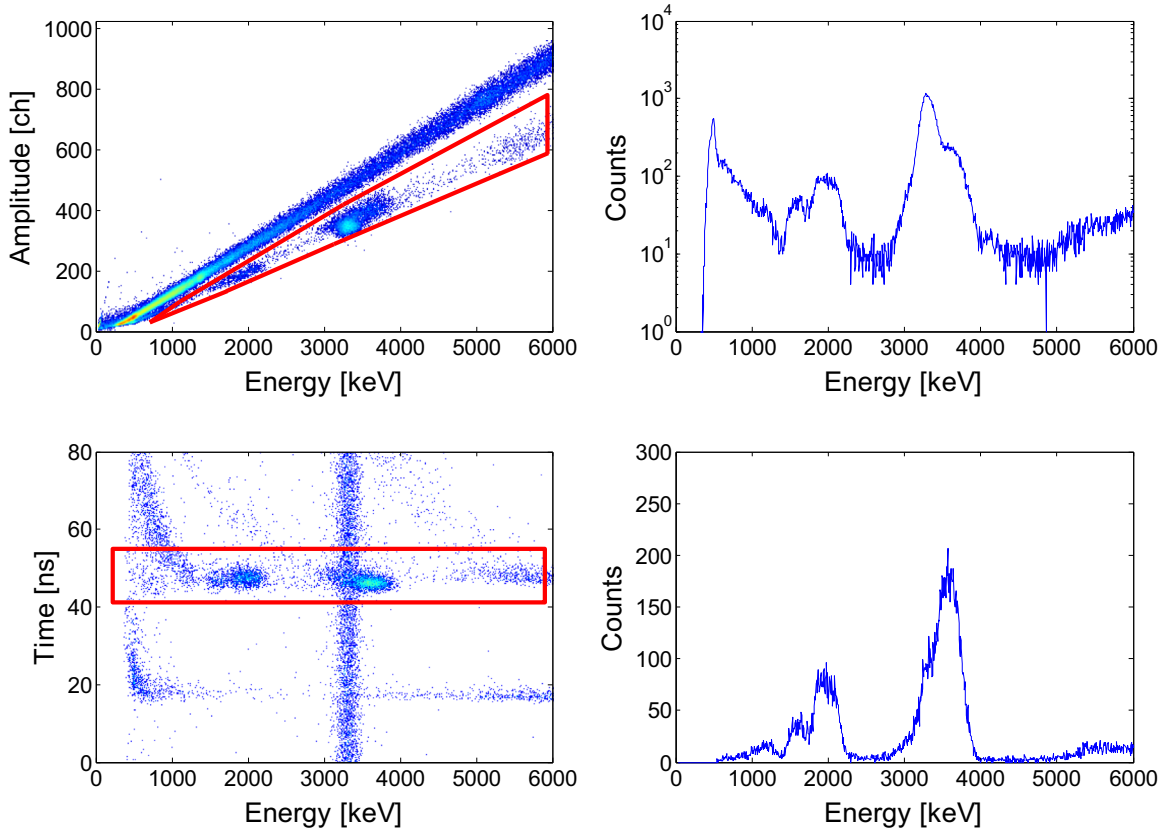

Fig. 12. In all panels, the CLYC-6 detector was placed at 0° and the beam energy was 5 MeV. Top-left panel: the amplitude vs energy matrix is shown. The red box is the graphical cut used to select the neutrons. The logarithm of the counts of the matrix is plotted on the *z* axis. Top-right panel: the energy spectrum obtained with the selection on neutrons in the amplitude vs energy matrix is shown. For the CLYC-6 detector, the dominant peak is the thermal neutron peak at ∼3.2 MeVee. Bottom left panel: the time vs energy matrix obtained gating on neutrons in the amplitude vs energy matrix. The red box indicates the gate on time used to obtain the energy spectrum shown in the bottom-right panel. The logarithm of the counts of the matrix is plotted on the *z* axis. Bottom-right panel: the fast neutron spectrum obtained with the two gates shown in the left top and bottom panels. The two peaks of the neutron capture on ^{35}Cl. (For interpretation of the references to color in this figure legend, the reader is referred to the web version of this article.)

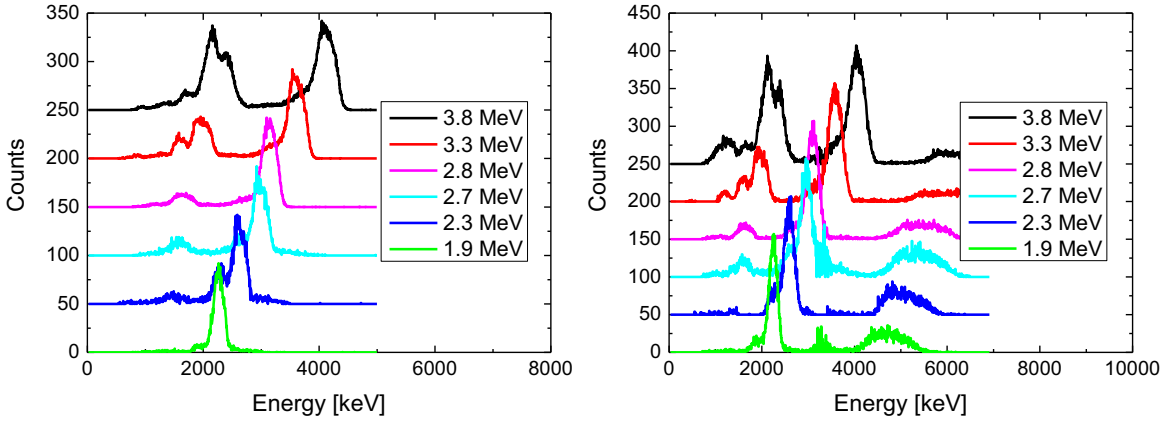

Fig. 13. The neutron spectra at the six different energies measured during the experiment are shown in left and right panel, for CLYC-7 and CLYC-6, respectively. The spectra were normalized at the maximum number of counts in the peak of ^{35}Cl(n,p)^{35}S reaction. A y-offset of 50 count was added to the curves corresponding to different neutron energies, for a better view. The neutron spectra were obtained with both the gate on the PSD ratio and the TOF. For the CLYC-6 detector the thermal neutron peak was subtracted.

allowing an easier separation between the neutrons induced reaction channels.

5. Conclusion

In this work, we investigated the possibility to use CLYC detectors in realistic nuclear physics experiments, where one needs to measure the energy spectrum of neutrons with unknown continuous energy in the MeV range. With this purpose, we combined the PSD and TOF techniques to disentangle both the contributions of neutrons with different energies and neutrons with the same energy undergoing different reaction channels.

The response of two CLYC scintillators (enriched with ∼95% of ^{6}Li and more than 99% of ^{7}Li) to fast neutrons (from 1.9 up to 3.8 MeV) was measured at the CN accelerator of LNL. A proton

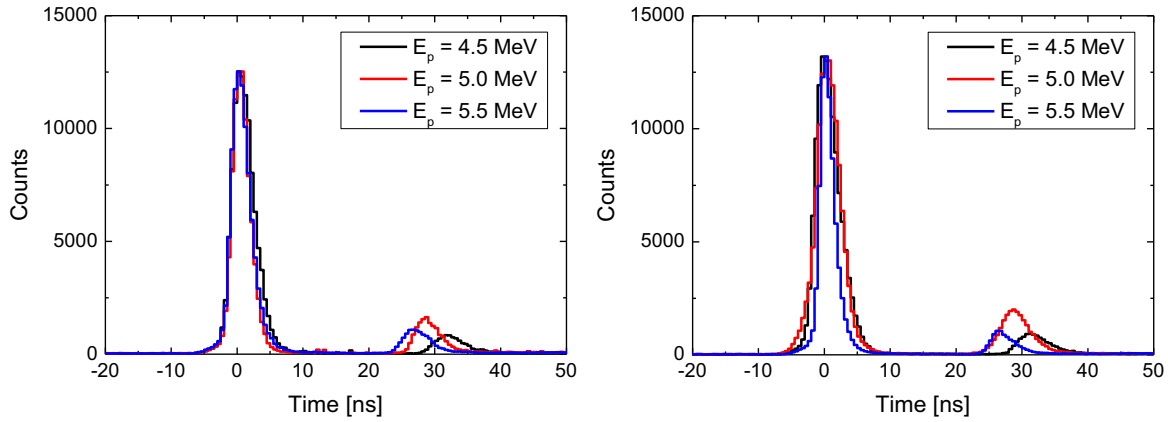

Fig. 14. The TOF spectra measured with CLYC-6 and CLYC-7 (left and right panel, respectively). The two detectors were placed at 0° degree. The time resolution varied from ~4.0 ns to ~6.5 ns owing to the beam time structure.

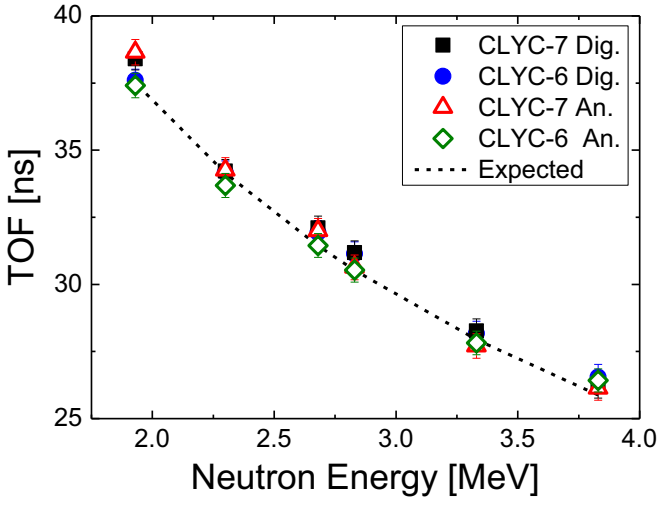

Fig. 15. The TOF measured for the six values of the neutron energy reported in Table 1. The TOF are plotted for both CLYC-6 (blue circles and green diamonds) and CLYC-7 (black squares and red triangles). The black dashed line represents the expected TOF for the fix distance between the detector and the target of 77 cm. (For interpretation of the references to color in this figure legend, the reader is referred to the web version of this article.)

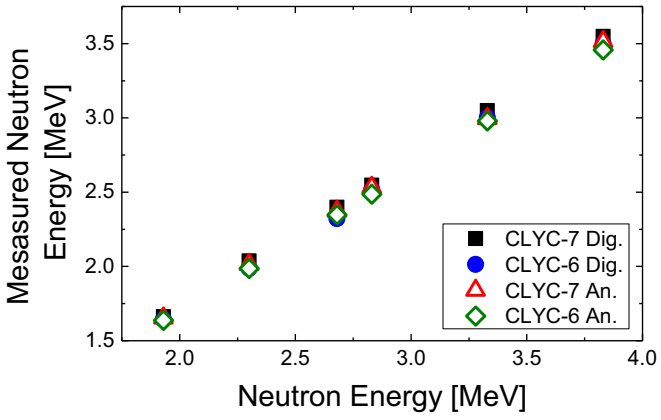

Fig. 16. The measured neutron energy after the subtraction of the Q-value of the reaction ^{35}Cl(n,p)^{35}S as a function of the expected neutron energy. The values reported are for both CLYC-6 (blue circles and green diamonds) and CLYC-7 (black squares and red triangles) and for both the analog (red triangles and green diamonds) and the digital (black squares and blue circles) acquisition system. (For interpretation of the references to color in this figure legend, the reader is referred to the web version of this article.)

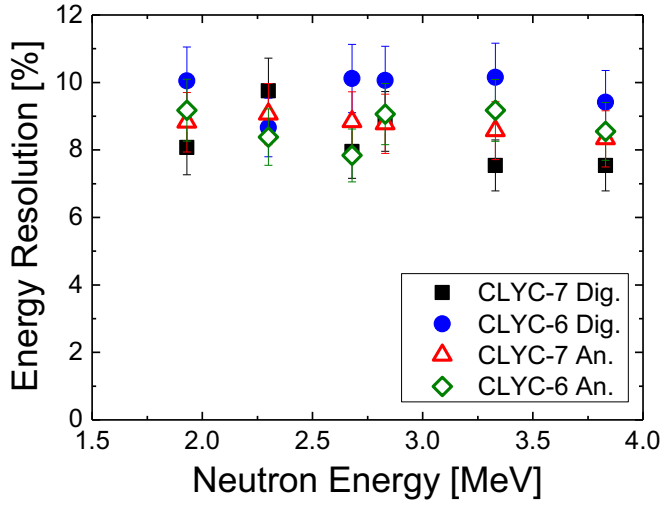

Fig. 17. The fast-neutron energy resolution measured with both CLYC-7 (black squares and red triangles) and CLYC-6 (blue circles and green diamonds) and for both analog (red triangle and green diamonds) and digital (black squares and blue circles) acquisition system. The energy resolution ranges between 7.5% and 10.2%. (For interpretation of the references to color in this figure legend, the reader is referred to the web version of this article.)

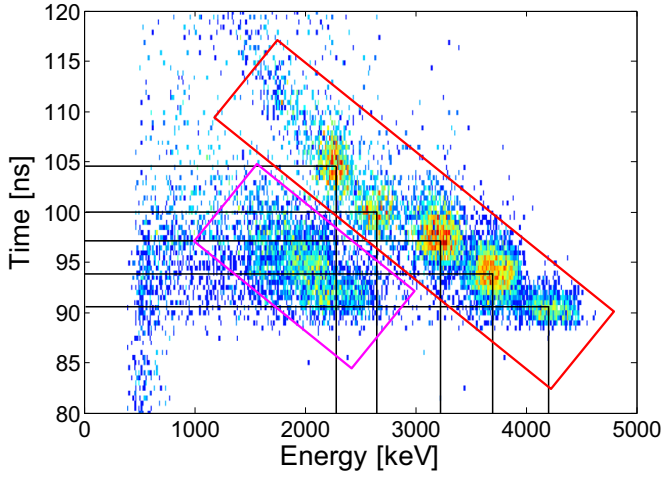

Fig. 18. The sum time vs energy matrixes (five of the six measured energy were selected) measured with the CLYC-7 detector. It is possible to see five different spots corresponding to detected neutrons. The red box is related to the neutrons detected with the reaction ^{35}Cl(n,p)^{35}S, while the magenta one to the neutron detected with the reaction ^{35}Cl(n,α)^{32}P. The logarithm of the counts of the matrix is plotted on the *z* axis. (For interpretation of the references to color in this figure legend, the reader is referred to the web version of this article.)

beam (of 4.5, 5.0 and 5.5 MeV) was accelerated on a thick ^{7}LiF target (700 μg/cm^{2}) to produce neutrons with different energies. The detectors were placed at 0° and at 90° to measure two neutron energies for each proton energy. Six different neutron energies were measured with both detectors. The beam was pulsed allowing to measure the TOF for an independent fast neutron energy measurement.

Two different acquisition systems were used: a digital acquisition system and an analog one. The results of the two acquisition systems were discussed and compared. The digital system allows a better separation between gamma rays and neutrons at low energies, but in general the fast neutron spectra measured with both acquisition systems are comparable.

The kinetic energy of fast neutrons was measured both via the energy signal and TOF. The fast-neutron energy resolution measured using the energy signal was found to range between 7.5% and 10.2%, for both detectors.

The measurement of TOF becomes fundamental for the CLYC-6 detector. Indeed, exploiting TOF it is possible to subtract the thermal neutron contribution (which represents a background for fast neutron measurement).

The combination of the two techniques greatly improves the CLYC scintillator neutron detection capability. In particular, the different reaction channels (for example protons and alpha particles emitted by the neutron-capture reactions on ^{35}Cl) can be separated. The possibility to identify the different reaction channels will be crucial in case of a continuum neutron spectrum. The CLYC-7 detector turns out to be a good neutron spectrometer in the studied energy range, whereas for CLYC-6 the neutron spectrum in the energy range of 3–3.5 MeV is dominated by the thermal neutron background, so that the TOF is fundamental for the subtraction of thermal neutrons.

Acknowledgments

We thank the CN accelerator staff for providing good quality pulsed beams. In particular the support of L. Maran, E. Munaron and L. Pranovi and is strongly acknowledged. This work was supported by NuPNET – ERA-NET within the the NuPNET GANAS project, under Grant agreement no. 202914 and from the European Union, within the “7th Framework Program” FP7/2007-2013, under Grant agreement no. 262010 – ENSAR-INDESYS. This work was also supported by “Programmi di Ricerca Scientifica di Rilevante Interesse Nazionale (PRIN)” No. 2001024324_01302. This work was also supported by the tecnological transfert agreement and scientific collaboration between INFN (Istituto nazionale di Fisica Nucleare), Italy and CAEN, Viareggio, Italy (TTB15MI005).

References

[1] BrilLanCe Scintillators Performance Summary.pdf, Available at: ⟨http://www.detectors.saint-gobain.com/Brillance380.aspx⟩.
[2] A. Giaz, et al., Nucl. Instrum. Methods A 729 (2013) 910–921.
[3] N. Cherepy, et al., IEEE Trans. Nucl. Sci. 60 (2013) 955.
[4] F. Quarati, et al., Nucl. Instrum. Methods A 729 (2013) 596.
[5] A. Giaz, et al., Nucl. Instrum. Methods A 804 (2015) 212–220, and references therein.
[6] (a) J. Glodo, et al., IEEE Trans. Nucl. Sci. 55 (2008) 1206; (b) J. Glodo, et al., IEEE Trans. Nucl. Sci. 56 (2009) 1257.
[7] J. Glodo, et al., IEEE Trans. Nucl. Sci. 58 (2011) 333.
[8] J. Glodo, et al., J. Cryst. Growth 79 (2013) 73.
[9] B.S. Budden, et al., IEEE Trans. Nucl. Sci. 60 (2013) 946.
[10] D.W. Lee, et al., Nucl. Instrum. Methods A 664 (2012) 1.
[11] M.M. Bourne, et al., Nucl. Instrum. Methods A 736 (2014) 124.
[12] M.B. Smith, et al., Nucl. Instrum. Methods A 784 (2015) 162.
[13] D'Olympia, et al., Nucl. Instrum. Methods A 694 (2012) 140.
[14] N. D'Olympia, et al., Nucl. Instrum. Methods A 714 (2013) 121.
[15] N. D'Olympia, et al., Nucl. Instrum. Methods A 763 (2014) 433.
[16] K. Yang, P. Menge, Nucl. Instrum. Methods A 784 (2015) 74.
[17] M.B. Smith, et al., Trans. Nucl. Sci. 60 (2013) 855.
[18] R. Machrafi, et al., Radiat. Meas. 70 (2014) 5.
[19] R.S. Woolf, et al., Nucl. Instrum. Methods A 803 (2015) 47.
[20] O. Wielnad, et al., Phys. Rev. Lett. 102 (2009) 092502.
[21] A. Giaz, et al., Phys. Rev. C 90 (2014) 014609.
[22] S. Ceruti, et al., Phys. Rev. Lett. 115 (2015) 222502.
[23] A. Giaz, et al., Nucl. Instrum Meth. A 810 (2016) 132.
[24] Pointwise ENDF-VII library at 300 K, ⟨http://atom.kaeri.re.kr⟩.
[25] G.F. Knoll, Radiation Detection and Measurement, Second ed., John Wiley & Sons, New York 1979, p. 484.
[26] C. Boiano, et al., IEEE NSS and MIC Conference Record, 2010, pp. 268.
[27] S. Brambilla, et al., IEEE NNS and MIC Conference Record, 2012, pp. 1087.